



Published in final edited form as:

Nature. 2013 April 11; 496(7444): 224–228. doi:10.1038/nature12041.

## Distinct extended amygdala circuits for divergent motivational states

Joshua H. Jennings<sup>1,2,\*</sup>, Dennis R. Sparta<sup>1,3,\*</sup>, Alice M. Stamatakis<sup>1,2</sup>, Randall L. Ung<sup>1</sup>, Kristen E. Pleil<sup>3,4</sup>, Thomas L. Kash<sup>2,3,4,5</sup>, and Garret D. Stuber<sup>1,2,3,5,6,#</sup>

<sup>1</sup>Department of Psychiatry, University of North Carolina at Chapel Hill, Chapel Hill, NC 27599

<sup>2</sup>Neurobiology Curriculum, University of North Carolina at Chapel Hill, Chapel Hill, NC 27599

<sup>3</sup>Bowles Center for Alcohol Studies, University of North Carolina at Chapel Hill, Chapel Hill, NC 27599

<sup>4</sup>Department of Pharmacology, University of North Carolina at Chapel Hill, Chapel Hill, NC 27599

<sup>5</sup>Neuroscience Center, University of North Carolina at Chapel Hill, Chapel Hill, NC 27599

<sup>6</sup>Department of Cell Biology and Physiology, University of North Carolina at Chapel Hill, Chapel Hill, NC 27599

### Summary

The comorbidity of anxiety and dysfunctional reward processing in illnesses such as addiction<sup>1</sup> and depression<sup>2</sup> suggests that common neural circuitry contributes to these disparate neuropsychiatric symptoms. The extended amygdala, including the bed nucleus of the stria terminalis (BNST), modulates fear and anxiety<sup>3,4</sup>, but also projects to the ventral tegmental area (VTA)<sup>5,6</sup>, a region implicated in reward and aversion<sup>7–13</sup>, thus providing a candidate neural substrate for integrating diverse emotional states. However, the precise functional connectivity between distinct BNST projection neurons and their postsynaptic targets in the VTA, as well as the role of this circuit in controlling motivational states have not been described. Here, we recorded and manipulated the activity of genetically and neurochemically identified VTA-projecting BNST neurons in freely behaving mice. Collectively, aversive stimuli exposure produced heterogeneous firing patterns in VTA-projecting BNST neurons. In contrast, *in vivo* optically-identified glutamatergic projection neurons displayed a net enhancement of activity to aversive stimuli, whereas the firing rate of identified GABAergic projection neurons was suppressed. Channelrhodopsin-2 (ChR2) assisted circuit mapping revealed that both BNST glutamatergic and GABAergic projections preferentially innervate postsynaptic non-dopaminergic VTA neurons, thus providing a mechanistic framework for *in vivo* circuit perturbations. *In vivo*

Users may view, print, copy, download and text and data-mine the content in such documents, for the purposes of academic research, subject always to the full Conditions of use: [http://www.nature.com/authors/editorial\\_policies/license.html#terms](http://www.nature.com/authors/editorial_policies/license.html#terms)

#Address correspondence to: Garret D. Stuber, Ph.D., Assistant Professor, Departments of Psychiatry & Cell Biology and Physiology, UNC Neuroscience Center, University of North Carolina at Chapel Hill, Tel: +1 (919) 843-7140, Fax: +1 (919) 966-1050, [gstuber@med.unc.edu](mailto:gstuber@med.unc.edu).

\*These authors contributed equally to this work

### Author contributions

D.R.S., J.H.J., and G.D.S. designed all experiments and wrote the manuscript. All authors collected, analyzed, and discussed the data.

photostimulation of BNST glutamatergic projections resulted in aversive and anxiogenic behavioral phenotypes. In contrast, activation of BNST GABAergic projections produced rewarding and anxiolytic phenotypes, which were also recapitulated by direct inhibition of VTA GABAergic neurons. These data demonstrate that functionally opposing BNST to VTA circuits regulate rewarding and aversive motivational states and may serve as a critical circuit node for bidirectionally normalizing maladaptive behaviors.

---

The ventral BNST (BNST<sub>v</sub>) is a heterogeneous structure<sup>14</sup> that innervates the VTA<sup>5,15–18</sup>, and aversive and rewarding stimuli activate a subset of these BNST<sub>v</sub> projection neurons<sup>19–21</sup>. To identify and record the activity of BNST<sub>v</sub>→VTA neurons using antidromic photostimulation *in vivo*, we targeted ChR2-eYFP22 under the control of a CaMKIIa promoter to the BNST<sub>v</sub> of adult mice. 4 – 6 weeks later, ChR2-eYFP was observed in BNST<sub>v</sub> cell bodies and projection fibers that innervate the VTA (Fig. 1a). Under anesthesia, optical fibers for antidromic photostimulation were positioned above the VTA, while recording electrodes and optical fibers for orthodromic photostimulation were positioned in the BNST<sub>v</sub> (Fig. 1b). We recorded from BNST<sub>v</sub> units that displayed reliable spiking to both orthodromic and antidromic-photostimulation. By systematically decreasing the interval between orthodromic- and antidromic-photostimulation, the fidelity of antidromic spikes was significantly attenuated (Fig. 1c,d), demonstrating spike collision<sup>23</sup>. In addition, antidromic spike latencies were significantly greater and showed less variability compared to orthodromic spikes (Fig. 1e,f), and antidromic spike fidelity was significantly greater than orthodromic spike fidelity to 40 Hz photostimulation (Fig. 1g). Thus, photostimulation of BNST<sub>v</sub>→VTA projections results in antidromic spiking that is reliably distinguishable from putative trans-synaptic circuit activation.

To examine the neurophysiological dynamics of identified BNST<sub>v</sub>→VTA neurons in behaving mice we implanted 16-channel multielectrode arrays in the BNST<sub>v</sub> as well as optical fibers above the VTA for antidromic identification of neurons<sup>24</sup> (Fig. 1h; Supplementary Fig. 1). Delivery of single 5 ms, 473 nm light pulses to the VTA resulted in time-locked firing in many BNST<sub>v</sub> neurons. Photostimulation of BNST<sub>v</sub>→VTA fibers resulted in a bimodal firing pattern in BNST<sub>v</sub> neurons due to distinguishable antidromic and polysynaptic activity (Supplementary Fig. 2, Supplementary Methods). Principle component and correlation analysis comparing waveform shapes demonstrated that spontaneous waveforms were highly correlated with light-evoked waveforms (average  $r = 0.950 \pm 0.008$ ; Supplementary Fig. 2; Supplementary Table 1)<sup>7</sup>. Light-evoked spike latencies revealed that a subset of recorded units consistently displayed time-locked spiking on  $11.21 \pm 0.68$  out of 20 trials (56%) with a mean latency of  $7.31 \pm 0.32$  ms (Fig. 1i,j), comparable with our anesthetized recording data (Fig. 1e), and a previous study using electrical antidromic stimulation of BNST projections in rodents<sup>25</sup>. Accordingly, neurons that were identified as antidromic-responsive displayed spike fidelity of  $81 \pm 15\%$  in response to 20 Hz photostimulation (Supplementary Fig. 2). Using these criteria (Supplementary Methods), we identified 53/137 units as BNST<sub>v</sub>→VTA projection neurons.

BNST<sub>v</sub> neurons display heterogeneous responses following aversive stimuli exposure<sup>19,20</sup>. Thus, we classified the firing patterns of identified BNST<sub>v</sub>→VTA neurons in response to

unpredictable foot shocks and associated contextual cues (Supplementary Methods). Identified BNSTv→VTA neurons segregated into three functionally distinct classes based on changes in their normalized firing rates throughout the foot-shock session (Supplementary Fig. 3), demonstrating that BNSTv→VTA neurons differentially encode information related to aversive stimuli and their associated contextual cues.

Electrical stimulation of the BNST produces both excitatory and inhibitory responses in VTA neurons *in vivo* implying that distinct subcircuits may exist. In mice injected with AAV5-CaMKIIa-ChR2-eYFP to nonspecifically target BNSTv→VTA projection neurons (CaMKIIa<sup>BNSTv→VTA::ChR2</sup>), whole-cell recordings in brain slices revealed that photostimulation of the CaMKIIa<sup>BNSTv→VTA</sup> pathway produced both glutamatergic and  $\gamma$ -aminobutyric acid (GABAergic) currents in VTA neurons (Supplementary Fig. 4), demonstrating that neurochemically distinct BNSTv neurons project to the VTA.

We next dissected the functional connectivity between distinct glutamatergic and GABAergic BNSTv→VTA neurons and their genetically defined postsynaptic targets within the VTA. Injection of a cre-inducible viral construct coding for ChR2-eYFP into the BNSTv in *Vglut2-ires-cre* or *Vgat-ires-cre* mouse lines<sup>26</sup> resulted in robust expression in the BNSTv as well as in fibers originating from these neurons that innervated the VTA (Fig. 2a,b). Whole-cell recordings from VTA neurons revealed that photostimulation of ChR2-containing fibers originating from *Vglut2* (*Vglut2*<sup>BNSTv→VTA::ChR2</sup>) or *Vgat* (*Vgat*<sup>BNSTv→VTA::ChR2</sup>) expressing BNSTv neurons produced excitatory or inhibitory postsynaptic currents respectively (Fig. 2c,d; Supplementary Fig. 5). *Vglut2*<sup>BNSTv→VTA</sup> and *Vgat*<sup>BNSTv→VTA</sup> terminals formed functional synapses primarily onto non-dopaminergic and medially located dopaminergic neurons, which have been implicated in responding to aversive stimuli<sup>7,9,11,13</sup> (Fig. 2e,f; Supplementary Fig 6–7; Supplementary Methods). These data provide a circuit blueprint by which BNSTv subcircuits interface with VTA-reward circuitry.

We next explored whether glutamatergic or GABAergic subpopulations of BNSTv→VTA neurons differentially respond to foot-shock sessions and associated contextual cues. Using optical antidromic activation *in vivo*, we identified 34/145 *Vglut2*<sup>BNSTv→VTA::ChR2</sup> expressing neurons (Supplementary Fig. 1; Supplementary Fig. 8; Supplementary Table 1). While all projection neurons displayed heterogeneous firing patterns (Supplementary Fig. 3), identified *Vglut2*<sup>BNSTv→VTA</sup> projection neurons exhibited a net enhancement of firing during the aversive event (Fig. 3a,b). In contrast, 33/77 identified *Vgat*<sup>BNSTv→VTA::ChR2</sup> expressing neurons principally exhibited reduced firing during the aversive event (Fig. 3c,d; Supplementary Fig. 1; Supplementary Fig. 8; Supplementary Table 1). In addition, 1 week after 5 consecutive daily foot-shock sessions, re-exposure to shock-associated contextual cues alone resulted in a net enhancement of *Vglut2*<sup>BNSTv→VTA::ChR2</sup> neuronal activity (Fig. 3e,f; Supplementary Fig. 9) while the activity of *Vgat*<sup>BNSTv→VTA::ChR2</sup> neurons were largely suppressed (Fig. 3g,h; Supplementary Fig. 9). Collectively, exposure to the aversive event or associated cues alone enhanced the firing of *Vglut2*<sup>BNSTv→VTA</sup> neurons, while simultaneously suppressing the activity of *Vgat*<sup>BNSTv→VTA</sup> neurons.

Since aversive stimuli enhanced the activity of  $Vglut2^{BNSTv \rightarrow VTA}$  neurons (Fig. 3a,b,e,f), which can excite non-dopaminergic VTA neurons (Fig. 2e), we next explored the behavioral consequences of selectively activating this projection in behaving mice. We tested mice in a real-time place preference paradigm to assay the effects of photostimulation of the  $Vglut2^{BNSTv \rightarrow VTA}$  pathway on motivational valence. Photostimulation of  $Vglut2^{BNSTv \rightarrow VTA}::ChR2$  mice resulted in a significant avoidance of a stimulation-paired chamber (Fig. 4a,b; Supplementary Figs. 10 and 11). Activation of this pathway also reduced active reward seeking (Supplementary Fig. 11). The aversive effects of this stimulation were dependent on local VTA glutamatergic signaling as infusions of an ionotropic glutamate receptor antagonist cocktail abolished the aversive phenotype induced by  $Vglut2^{BNSTv \rightarrow VTA}$  activation (Fig. 4b; Supplementary Fig. 12 and 13). In addition, inescapable activation of this pathway for 20 min in an open field resulted in significantly less center- and more corner-time in  $Vglut2^{BNSTv \rightarrow VTA}::ChR2$  mice in the 10 min following stimulation offset compared to controls, suggesting that enhanced activity in the  $Vglut2^{BNSTv \rightarrow VTA}$  pathway contributes to anxiety-like behavior (Fig. 4c; Supplementary Fig. 11).

In contrast to the aversive consequences of stimulating the  $Vglut2^{BNSTv \rightarrow VTA}$  pathway, 20 Hz photostimulation in  $Vgat^{BNSTv \rightarrow VTA}::ChR2$  mice resulted in a significant place preference (Fig. 5a,b; Supplementary Figs. 10 and 14). VTA infusions of a GABA<sub>A</sub> receptor antagonist prevented the  $Vgat^{BNSTv \rightarrow VTA}$  mediated place preference compared to saline injections (Fig. 5b; Supplementary Figs. 12 and 13). To determine if *in vivo* optogenetic activation of the  $Vgat^{BNSTv \rightarrow VTA}$  pathway produces active reward seeking, we tested whether these mice would nose poke to receive photostimulation<sup>27</sup>.  $Vgat^{BNSTv \rightarrow VTA}::ChR2$  mice readily nose poked to receive photostimulation (Fig. 5c; Supplementary Fig. 14). Together, these data suggest that photostimulation of the  $Vgat^{BNSTv \rightarrow VTA}$  pathway promotes reward-related behaviors.

Since the  $Vgat^{BNSTv \rightarrow VTA}$  projection preferentially innervates non-dopaminergic VTA neurons (Fig. 2f), we considered VTA GABAergic neurons as the likely postsynaptic target. VTA GABAergic neuronal inhibition via halorhodopsin activation ( $Vgat^{VTA}::NpHR$ ; Supplementary Figs. 15 and 16) also produced reward-related phenotypes (Fig. 5d,e,f). Together, these results show that reward-related responses to  $Vgat^{BNSTv \rightarrow VTA}$  activation are recapitulated by directly inhibiting  $Vgat^{VTA}$  neurons, thus providing a circuit mechanism for the  $Vgat^{BNSTv \rightarrow VTA}$  pathway to regulate motivated behavior.

Since the BNST regulates the expression of fear and anxiety-related behavioral phenotypes<sup>3,28,29</sup>, we also sought to establish a role for the  $Vgat^{BNSTv \rightarrow VTA}$  pathway in these negative motivational states. Photostimulation of the  $Vgat^{BNSTv \rightarrow VTA}$  pathway and direct inhibition of  $Vgat^{VTA}$  neurons significantly increased time spent in the open arms of an elevated plus maze, indicative of anxiolysis (Fig. 5g; Supplementary Fig. 17). These coinciding observations suggest that  $Vgat^{BNSTv \rightarrow VTA}$  and  $Vgat^{VTA}$  neurons serve as critical circuit nodes for moderating the expression of anxiety.

Given that  $Vgat^{BNSTv \rightarrow VTA}$  neurons are largely inhibited by aversive stimuli (Fig. 3c,d,g,h), we examined whether concurrent activation of the  $Vgat^{BNSTv \rightarrow VTA}$  projection during an

unpredictable foot-shock session could alleviate the subsequent development of anxiety-like behavior. Immediately following termination of the foot-shock session and cessation of *Vgat*<sup>BNSTv→VTA::ChR2</sup> stimulation, we measured the acute freezing response while still in the shock-associated context, as well as behavior in the elevated-plus maze 3 hr later (Supplementary Fig. 18; Supplementary Methods). *Vgat*<sup>BNSTv→VTA::ChR2</sup> mice spent significantly less time frozen (Fig. 5h), as well as significantly more open-arm time and entries in the elevated-plus maze relative to controls (Supplementary Fig. 18). Taken together, these data suggest that enhancing activity of the *Vgat*<sup>BNSTv→VTA</sup> pathway during aversive stimuli exposure has anxiety-buffering properties. While the canonical view of BNST function proposes a dominant role of this structure in promoting anxiety states<sup>3,4,30</sup>, the cellular and functional complexity described here (Supplementary Fig. 19) illustrates that particular BNST circuit elements orchestrate divergent aspects of emotional and motivational processing.

## Methods summary

All procedures were conducted in accordance with the Guide for the Care and Use of Laboratory Animals, as adopted by the NIH, and with approval of the Institutional Animal Care and Use Committee at UNC and described in detail in the Supplementary Methods.

## Online methods

### Experimental subjects and stereotactic surgery

All procedures were conducted in accordance with the Guide for the Care and Use of Laboratory Animals, as adopted by the NIH, and with approval of the Institutional Animal Care and Use Committee at UNC. Adult (25–30g) male C57BL/6J mice (Jackson Laboratory), adult male *Vgat-ires-cre* mice and adult male *Vglut2-ires-cre* mice (see 26 for additional details on the *Vglut2-ires-cre* and *Vgat-ires-cre* mouse lines) were group housed prior to surgery. All mice were maintained on a reverse 12 hr light cycle (lights off at 07:00) with *ad libitum* access to food and water, unless described below. Mice were anesthetized with a ketamine (150 mg per kg of body weight) and xylazine (50 mg per kg) solution and placed into a stereotactic frame (Kopf Instruments). For all *in vivo* electrophysiology experiments, male mice were unilaterally injected with 0.5  $\mu$ l of purified and concentrated adeno-associated virus (AAV) ( $\sim$ 10<sup>12</sup> infections units per ml, packaged and titered by the UNC Vector Core Facility) into the BNSTv using the following stereotactic coordinates: + 0.14 mm to bregma,  $\pm$  0.9 lateral to midline, and – 4.8 mm ventral to the skull surface. All viral constructs were packaged by the UNC vector core facility at a final working concentration of 1 – 5E12 genome copies per mL.

For all *in vivo* electrophysiology experiments, mice were implanted with a 16-wire (4  $\times$  4 configuration, wire diameter  $\sim$ 30 $\mu$ m) tungsten multielectrode array (MEA) (Innovative Neurophysiology, Inc) aimed at the BNSTv using the stereotactic coordinates stated above. For all *in vivo* electrophysiological and *in vivo* behavioral experiments, except for the VTA microinjection experiments, all mice were implanted with an optical fiber aimed at the VTA (see 24 for additional details) using the following stereotactic coordinates: –3.2 mm to bregma,  $\pm$ 0.5 lateral to midline, and –4.69 mm ventral to skull surface. For the VTA

microinjection experiments, a 26-gauge steel tube cannula (McMasters-Carr) that terminated 0.5 mm above the tip of the optical fiber was epoxied to an optical fiber and unilaterally aimed at the VTA using the following stereotactic coordinates: -3.2 mm to bregma, +/-0.5 lateral to midline, and -4.69 mm ventral to skull surface. For photoinhibition of VTA-GABAergic neurons using NpHR3.0, all mice were bilaterally implanted with an optical fiber at a 10° angle in the VTA using the following stereotactic coordinates: -3.2 mm to bregma, +/-1.1 lateral to midline, and -4.75 mm ventral to skull surface. The time from virus injection to the start of the experiments was 4 – 6 weeks for all ChR2 terminal stimulation manipulations and 3 – 4 weeks for cell body manipulations.

### **Histology, immunohistochemistry, and microscopy**

Mice were anesthetized with pentobarbital and transcardially perfused with phosphate buffered saline (PBS) followed by 4% paraformaldehyde (weight/volume) in PBS. 40 µm brain sections were subjected to immunohistochemical staining for neuronal cell bodies (NeuroTrace Invitrogen; 640 nm excitation/660 nm emission or 435 nm excitation/455 nm emission and/or tyrosine hydroxylase (TH)) (Pel Freeze; made in sheep, 1:500) (see<sup>10,13</sup> for additional information). Brain sections were mounted, coverslipped, and z-stack and tiled images were captured on a Zeiss LSM 710 confocal microscope using a 20x or 63x objective. To determine optical fiber placement, tissue was imaged at 10x and 20x on an upright epi-fluorescent microscope.

### ***In vivo* anesthetized electrophysiology**

C57BL/6J mice were bilaterally injected with 0.3 µl of AAV5-CaMKIIa-ChR2-eYFP into the BNSTv. 6 weeks following virus injection, mice were anesthetized with 0.5 – 1.0% isoflurane (Butler Schein) and were placed into a stereotaxic frame (Kopf Instruments). Body temperature was maintained at ~ 37°C with a homeothermic heating blanket (Harvard Apparatus, Holliston, MA). Tail pinches were administered frequently to monitor responses under anesthesia. A reference electrode was fixed inside brain tissue, approximately 2 mm from both the BNSTv and VTA. Extracellular neural activity was recorded using a glass recording electrode (5 – 10 MΩ; and filled with 0.5 M NaCl). The recording electrode was lowered into the BNSTv (+ 0.14 mm to bregma, +/- 0.9 lateral to midline, and - 4.8 mm ventral to the skull surface) by a motorized micromanipulator (Scientifica). Recordings were amplified (Multiclamp 700B, Molecular Devices), highpass filtered at 6 kHz and sampled at 10 kHz. Here, orthodromic photostimulation refers to action potentials initiated at the cell body, while antidromic photostimulation refers to backward propagating action potentials initiated at distal axonal fibers; both are independent of synaptic transmission.

For orthodromic activation, an optical fiber coupled to a solid state laser (473 nm) was fed through the side port of the electrode holder to terminate near the tip of the glass recording electrode, which allowed for delivery of ~5 mW light pulses into the BNSTv. For antidromic activation, an optical fiber housed in a steel cannula and coupled to a separate solid state laser (473 nm) was inserted into the VTA at a 16° angle (- 3.2 mm to bregma, + 1.4 mm lateral to midline, and - 4.9 mm ventral to the skull surface), which delivered ~10 mW of light to the VTA. BNSTv neurons were classified as antidromic-responsive, if the following 3 criteria were met: 1) stable antidromic spike latency (< 0.2 ms), 2) ability to

respond reliably to high frequency photostimulation, 3) collision between orthodromic- and antidromic-evoked spikes. Each photostimulation parameter delivered a 5 ms light pulse to either BNSTv cell bodies (orthodromic) or BNSTv axons within the VTA (antidromic). To determine stable antidromic latencies, 5 ms light pulses were delivered to the VTA every 5 s for 20 trials. To confirm reliable antidromic spike fidelity, 20, 40, and 100 Hz train pulses of light were delivered to the VTA every 10 s for 10 trials at each frequency. To validate spike collision, we varied the collision interval (0, 1, 2, 5, 10, 20 ms) between orthodromic and antidromic photostimulation. Each collision interval was repeated every 5 s for a total of 10 trials. Data acquisition and analysis was performed using pCLAMP software (Molecular Devices). Placements of recording electrode tips within the BNSTv and optical fibers within the VTA were verified with histological examination of brain tissue following the experiments.

### Patch-clamp electrophysiology

Brain slices preparation and general methods for patch-clamp electrophysiology were conducted as previously described<sup>10,13</sup>, with the following changes. To examine both BNSTv postsynaptic glutamatergic and GABAergic currents, C57BL/6J mice were injected with AAV5-CaMKIIa-ChR2-eYFP to nonspecifically target BNSTv→VTA projection neurons (CaMKIIa<sup>BNSTv→VTA::ChR2</sup>). For whole-cell voltage recordings (EPSCs and IPSCs) from VTA neurons, electrodes (2–4 M $\Omega$  electrode resistance) contained in mM: 117 cesium methanesulfonate, 20 HEPES, 0.4 EGTA, 2.8 NaCl, 5 TEA, 2 Mg-ATP, 0.2 Na-GTP (pH 7.2–7.4), 275–285 mOsm. The cesium methanesulfonate internal solution also contained the selective NMDA antagonist, MK-801 (1.125 mM). VTA neurons were held at  $V_h = -70$  mV ( $E_{REV}$  for GABA<sub>A</sub> receptors) and  $V_h = +10$  mV ( $E_{REV}$  for AMPA receptors) to examine both glutamatergic and GABAergic postsynaptic currents respectively within the same neuron. Photostimulation (5 ms pulses of 1–2 mW, 473 nm light delivery via LED through a 40x microscope objective) was used at both voltages. In a subset of neurons ( $n = 4$  of 11 neurons), TTX (1  $\mu$ M) and 4-AP (1 mM) was bath applied to isolate monosynaptic currents.

To isolate BNSTv glutamatergic and GABAergic postsynaptic currents, *Vglut2*<sup>BNSTv→VTA::ChR2</sup> and *Vgat*<sup>BNSTv→VTA::ChR2</sup> mice were used for recordings. For whole-cell voltage clamp recordings of VTA EPSCs from *Vglut2*<sup>BNSTv→VTA::ChR2</sup> mice, once stable light-evoked EPSCs were achieved, 10  $\mu$ M DNQX was bath applied. For whole-cell voltage clamp recordings of VTA IPSCs from *Vgat*<sup>BNSTv→VTA::ChR2</sup> mice, once stable light-evoked IPSCs were achieved, 10  $\mu$ M Gabazine was bath applied.

### Ex vivo validation of photoinhibition of VTA GABA neurons

For current clamp recordings to show hyperpolarization of membrane voltage from VTA GABA neurons following NpHR inhibition, *Vgat*-ires-cre mice were transduced with Cre-inducible NpHR under control of the EF1 $\alpha$  promoter in the VTA. Electrodes (2–4 M $\Omega$ ) contained in mM: 130 K-gluconate, 10 KCl, 10 HEPES, 10 EGTA, 2 MgCl<sub>2</sub>, 2 Mg-ATP, 0.2 Na-GTP (pH 7.2–7.4), 275–285 mOsm. VTA neurons were maintained at  $\sim -60$  mV. For photoinhibition, 500 ms pulses of 5–8 mW, 532 nm light delivery via a solid-state laser coupled to an optical fiber positioned in the brain slice.

## Unpredictable foot-shock paradigm

Mice were placed in sound-attenuated mouse behavioral chambers (Med Associates) where an unpredictable foot shock was used as an aversive stimulus. A houselight and white noise signaled the start of the trial and remained on throughout the entire 20 min foot-shock session (contextual cues). Each unpredictable foot shock was 0.75 mA in intensity and 500 ms in duration on a variable interval (VI60) schedule. Mice received approximately 20 unpredictable foot shocks during the entire 20 min session.

For the *in vivo* electrophysiology experiments, *Vglut2*<sup>BNSTv→VTA::ChR2</sup> and *Vgat*<sup>BNSTv→VTA::ChR2</sup> mice implanted with a MEA in the BNSTv and an optical fiber in the VTA were placed in the unpredictable foot-shock context where they received the visual and auditory contextual cues in the absence of foot shock for 20 min (contextual cue exposure prior to shock association). 5 days after the unpaired contextual cue session, mice were run in the standard unpredictable foot-shock session (approx. 20 unpredictable foot shocks, 0.75 mA, 500 ms) for 5 consecutive days as stated above, which included paired presentation of the contextual cues. 7 days following the 5<sup>th</sup> unpredictable foot-shock session, mice were placed back into the unpredictable foot-shock paradigm, where they received the visual and auditory contextual cues (houselight and white noise) in the absence of foot shock for 20 min.

## *In vivo* electrophysiology

Neural activity was recorded using an Omniplex recording system (Plexon Instruments). Signals from each electrode in the array were referenced to ground, and recordings were performed in differential mode to subtract artifacts unrelated to neural activity. Acquired data was bandpass filtered between 0.1 and 8,000 Hz. Spike sorting was performed offline using Offline sorter (Plexon Instruments), as previously described<sup>31,32</sup>. Briefly, discrimination of individual units was performed offline using principal component analysis to separate individual units from the same electrode. In addition, auto- and cross-correlograms, firing characteristics, and inter-spike interval distributions were examined to ensure units were well-isolated. In addition, timestamp data to signify the start and end of foot-shock sessions, and the delivery of light pulses to optical fibers was synchronized with electrophysiological data. Sorted waveforms were further processed in NeuroExplorer (Nex Technologies) to extract unit timestamps and relevant events. NeuroExplorer-extracted timestamps were exported to MATLAB and further data processing and statistical testing. Neuronal units were included in the data if the signal-to-noise ratio was high, and the mean firing rate was between 0.5 – 25 Hz during baseline recording periods. During the time epoch surrounding the individual delivered foot shocks, large shock artifact were readily apparent. While these were easily isolated and excluded from the analyzed waveform data using offline spike sorting, neuronal firing responses in the 500 – 1000 ms following foot shock onset could not be reliably quantified. Thus, data collected during these time epochs were excluded from analysis. This represents an approximate loss of 0.8 – 1.66% of the collected data during the foot-shock session. Resulting data was binned in 30 s epochs in order to minimize the skewing of our results due to data lost by the shock artifacts. In addition, recording sites was verified histologically using electrolytic lesions at 200  $\mu$ A for 5 s.

To identify units originating from BNSTv projection neurons, 5 ms light pulses were delivered to VTA to antidromically stimulate BNSTv projection neurons that innervated the area. Light pulses were delivered in 10 s intervals for 20 trials starting 40 min after the end of the unpredictable foot-shock session. Recorded BNSTv units were classified as light-responsive, and thus VTA-projecting, if they met both of the following two criteria. 1) The latency of the first spike after light stimulation onset was less than 20 ms for 20% of the trials. 2) Light-evoked and spontaneous waveform shapes had a correlation coefficient of > 0.90. To compare light-evoked and spontaneous waveforms from units, light-evoked waveform characteristics were defined using the average waveform shape and average principal component values (PC1–3) of the first spike following photostimulation onset from each successful trial where a waveform was collected within 20 ms after light onset. This subset of light-evoked waveforms were then averaged together for a given unit, and compared to a subset of spontaneous, non-light-evoked waveforms that occurred immediately preceding the onset of light stimulations (pre-stimulation waveforms) and the first collected waveforms occurring after the 20 ms interval following the offset of photostimulations (post-stimulation waveforms). The correlation between each average waveform shape over the three time epochs (pre-stimulation, during stimulation, post-stimulation) was then calculated using Pearson's product-moment coefficient as well as their average principle component values.

VTA-projecting BNSTv neuronal units were then further classified, dependent on their firing response to the foot shock session into 3 categories: foot-shock session-excited, foot-shock session-inhibited and foot-shock session-no effect. To clarify, foot-shock session-excited, foot-shock session-inhibited, and foot-shock session-no effect refers to a neural unit's activity in response to the collective aversive experience, not to individual foot shocks. To assess the firing rate of a particular neuron, each spike from 10 min preceding the foot shock session to 20 min following the end of the foot shock session was binned into 30 s bins. Firing rate was then normalized to the mean firing rate during the 10 min preceding the start of the 20 min foot-shock session using z-scores. Neurons were classified as foot-shock session-excited if their average z-score during the 20-min foot-shock session was greater than 1. Likewise, neurons were classified as foot-shock session-inhibited if their average z-score during the shock session fell below -1. All other units where the z-score did not exceed an absolute value of 1 during the 20 min foot-shock session were classified as no effect. Neural activity was recorded from the same mice during the cue exposure, foot shock, and cue re-exposure sessions, therefore we were able to reliably record activity from the same population of neurons during each of the three sessions.

### **Photostimulation of *Vglut2*<sup>BNSTv→VTA::ChR2</sup> and *Vgat*<sup>BNSTv→VTA::ChR2</sup> projections and photoinhibition of *Vgat*<sup>VTA::NpHR</sup> neurons during real-time place preference**

*Vglut2*<sup>BNSTv→VTA::ChR2</sup>, *Vgat*<sup>BNSTv→VTA::ChR2</sup>, *Vgat*<sup>VTA::NpHR</sup>, and litter mate controls were implanted with optical fibers above the VTA and were run in the real-time place preference paradigm. See10 for additional details on this method.

### Intra-VTA injection of antagonists and photostimulation of *Vglut2*<sup>BNSTv→VTA::ChR2</sup> and *Vgat*<sup>BNSTv→VTA::ChR2</sup> projections during real-time place preference

A separate cohort of *Vglut2*<sup>BNSTv→VTA::ChR2</sup> and *Vgat*<sup>BNSTv→VTA::ChR2</sup> mice were unilaterally implanted with a 26-gauge cannula coupled to an optical fiber aimed above the VTA. All mice were placed in a custom-made place preference arena and were run in the real-time place preference paradigm to achieve a baseline measurement. Two days following the baseline session, *Vglut2*<sup>BNSTv→VTA::ChR2</sup> mice were injected with either 0.3 μl of vehicle (saline) or a cocktail of selective glutamate antagonists (0.1 μg AP-5/0.001 μg DNQX in saline) and *Vgat*<sup>BNSTv→VTA::ChR2</sup> mice were injected with either 0.3 μl of vehicle (saline) or a selective GABA<sub>A</sub> antagonist (0.001 μg Gabazine) into the VTA in a counter balanced design (all drugs from Tocris). The injector needle (33 gauge steel tube, McMasters-Carr) extended approximately 1 mm past the cannula to ensure drug delivery 0.5 mm below the optical fiber. All mice were infused at a rate of 0.1 μl per minute. The injector remained in place for approximately 2 min following infusion to ensure proper diffusion of drug into the VTA. Immediately following the microinjection procedure, all mice were placed into the real-time place preference chamber. Mice had 2 days off between each VTA microinjection.

### Photostimulation of *Vglut2*<sup>BNSTv→VTA::ChR2</sup> projections during open-field testing

*Vglut2*<sup>BNSTv→VTA::ChR2</sup> and *Vglut2*<sup>BNSTv→VTA::Control</sup> mice were examined in a custom made open field arena (25 × 25 × 25 cm white plexiglass arena) for 35 min. After a baseline period of 5 min, all mice received constant 20 Hz photostimulation. Immediately, following the 20 min photostimulation epoch, all mice had a 10 min period in which they received no photostimulation. Center zone was defined as the center 156 cm<sup>2</sup> (25% of the entire arena). Corner zones were defined as the 39 cm<sup>2</sup> in each corner. The 35 min session was recorded with a CCD camera that was interfaced with Ethovision software (Noldus Information Technologies). Time spent in the corner and the center of the open-field apparatus was recorded. Heat maps and post-acquisition processing were conducted in MATLAB (Mathworks Inc.).

### Photostimulation of *Vglut2*<sup>BNSTv→VTA::ChR2</sup> projections during sucrose self-administration

*Vglut2*<sup>BNSTv→VTA::ChR2</sup> and *Vglut2*<sup>BNSTv→VTA::Control</sup> mice with optical fibers implanted above the VTA were first food restricted to 90% of their free-feeding weight. They were then placed in standard mouse operant chambers in order to nose poke for a 15% (w/v) sucrose solution on FR-1 schedule in a 30 min session. Once stable nose-poking behavior for 15% sucrose was observed (approx. 100 active nose pokes on at least 2 consecutive days), all mice received constant 20 Hz photostimulation during the entire 30 min sucrose session.

### Optical self-stimulation of *Vgat*<sup>BNSTv→VTA::ChR2</sup> projections

*Vgat*<sup>BNSTv→VTA::ChR2</sup> and *Vgat*<sup>BNSTv→VTA::Control</sup> mice with optical fibers implanted above the VTA were trained in one 30 min session to nose poke on a fixed ratio (FR-1) schedule for optical self-stimulation of the *Vgat*<sup>BNSTv→VTA::ChR2</sup> projections in standard

mouse operant chambers (Med Associates). Each nose poke resulted in a single 3 s 20 Hz optical pulse train. Following the 1 day 20 Hz training session, mice were run daily at each photostimulation frequency (1, 5, 10, 20, 40 Hz) in a counter-balanced design.

### Optical self-inhibition of *Vgat*<sup>VTA::NpHR</sup> neurons

*Vgat*<sup>VTA::NpHR</sup> and *Vgat*<sup>VTA::Control</sup> mice with optical fibers implanted above the VTA were trained in one 30 min session to nose poke on a fixed ratio (FR-1) schedule for photoinhibition of VTA GABAergic cell bodies in standard mouse operant chambers as described above (Med Associates).

### Photostimulation of *Vgat*<sup>BNSTv→VTA::ChR2</sup> projections and photoinhibition of *Vgat*<sup>VTA::NpHR</sup> neurons during the elevated plus maze

*Vgat*<sup>BNSTv→VTA::ChR2</sup>, *Vgat*<sup>VTA::NpHR</sup>, *Vgat*<sup>VTA::Control</sup>, and *Vgat*<sup>BNSTv→VTA::Control</sup> mice were run in the elevated plus maze (EPM) to assay anxiety-like behavior. Activity and location was recorded for 5 min (baseline). Following this 5 min baseline period, *Vgat*<sup>BNSTv→VTA::ChR2</sup> and *Vgat*<sup>BNSTv→VTA::Control</sup> mice received constant 20 Hz photostimulation for 5 min, while *Vgat*<sup>VTA::NpHR</sup> and *Vgat*<sup>VTA::Control</sup> mice received constant inhibition for 5 min. Immediately following the 5 min photostimulation or photoinhibition epoch, all mice had a 5 min period in which they received no light delivery.

### Photostimulation of *Vgat*<sup>BNSTv→VTA::ChR2</sup> projections during foot-shock followed by freezing and anxiety-like behavior measurements

*Vgat*<sup>BNSTv→VTA::ChR2</sup> and *Vgat*<sup>BNSTv→VTA::Control</sup> mice with optical fibers implanted above the VTA were run in a modified foot-shock paradigm as described above. Briefly, mice were placed into sound attenuated mouse chambers (Med Associates) for a 5 min baseline period. After the 5 min baseline period, a house light and white noise were activated and mice received the same foot shock protocol as described above. Additionally, during the 20 min shock session, all mice received constant 20 Hz photostimulation. A separate cohort of mice (*Vgat*<sup>BNSTv→VTA::ChR2</sup> and *Vgat*<sup>BNSTv→VTA::Control</sup>) received constant 20 Hz photostimulation of this pathway in the absence of foot shock. Immediately following the 20 min foot shock and photostimulation epoch, all mice had a 5 min period in which they received no foot shock or photostimulation while still exposed to contextual cues, to assay freezing behavior. Freezing was defined as the total lack of any movement, except respiration for a period of 2 s. The 30 min test session was recorded with a CCD camera that was interfaced with Ethovision software (Noldus Information Technologies). Time frozen during the 5 min period immediately following the foot shock and photostimulation session was recorded. Approximately 3 hr after the foot shock and photostimulation session or just the photostimulation session in the absence of foot shock, mice were run on the elevated-plus maze to assay anxiety-like behavior for 5 min.

## Supplementary Material

Refer to Web version on PubMed Central for supplementary material.

## Acknowledgments

We thank Malhar Patel, Jana Phillips, Scot Maciver, for assistance, Dr. Vladimir Gukassyan and the UNC Neuroscience Center Microscopy Core (P30 NS045892), and members of the Stuber lab for discussion. We thank Dr. Karl Deisseroth for viral constructs and the UNC vector core facility for viral packaging. We thank Drs. Bradford Lowell and Linh Vong for providing the *Vgat-ires-cre* and *Vglut2-ires-cre* mice. This study was supported by The Whitehall Foundation, The Foundation of Hope, and DA029325 and DA032750 (G.D.S.). D.R.S. was supported by (AA018610 and AA007573). A.M.S. was supported by (NS007431 and DA034472).

## References

1. Koob GF, Le Moal M. Drug addiction, dysregulation of reward, and allostasis. *Neuropsychopharmacology*. 2001; 24:97–129. [PubMed: 11120394]
2. Nestler EJ, Carlezon WA Jr. The mesolimbic dopamine reward circuit in depression. *Biol Psychiatry*. 2006; 59:1151–1159. [PubMed: 16566899]
3. Davis M, Walker DL, Miles L, Grillon C. Phasic vs sustained fear in rats and humans: role of the extended amygdala in fear vs anxiety. *Neuropsychopharmacology*. 2010; 35:105–135. [PubMed: 19693004]
4. Walker DL, Davis M. Role of the extended amygdala in short-duration versus sustained fear: attribute to Dr Lennart Heimer. *Brain Struct Funct*. 2008; 213:29–42. [PubMed: 18528706]
5. Geisler S, Zahm DS. Afferents of the ventral tegmental area in the rat-anatomical substratum for integrative functions. *J Comp Neurol*. 2005; 490:270–294. [PubMed: 16082674]
6. Georges F, Aston-Jones G. Potent regulation of midbrain dopamine neurons by the bed nucleus of the stria terminalis. *J Neurosci*. 2001; 21
7. Cohen JY, Haesler S, Vong L, Lowell BB, Uchida N. Neuron-type-specific signals for reward and punishment in the ventral tegmental area. *Nature*. 2012; 482:85–88. [PubMed: 22258508]
8. Fields HL, Hjelmstad GO, Margolis EB, Nicola SM. Ventral tegmental area neurons in learned appetitive behavior and positive reinforcement. *Annual review of neuroscience*. 2007; 30:289–316.
9. Lammel S, et al. Input-specific control of reward and aversion in the ventral tegmental area. *Nature*. 2012; 491:212–217. [PubMed: 23064228]
10. Stamatakis AM, Stuber GD. Activation of lateral habenula inputs to the ventral midbrain promotes behavioral avoidance. *Nat Neurosci*. 2012; 15:1105–1107. [PubMed: 22729176]
11. Tan KR, et al. GABA neurons of the VTA drive conditioned place aversion. *Neuron*. 2012; 73:1173–1183. [PubMed: 22445344]
12. Tye KM, et al. Dopamine neurons modulate neural encoding and expression of depression-related behaviour. *Nature*. 2013; 493:537–541. [PubMed: 23235822]
13. van Zessen R, Phillips JL, Budygin EA, Stuber GD. Activation of VTA GABA neurons disrupts reward consumption. *Neuron*. 2012; 73:1184–1194. [PubMed: 22445345]
14. Hammack SE, Mania I, Rainnie DG. Differential expression of intrinsic membrane currents in defined cell types of the anterolateral bed nucleus of the stria terminalis. *J Neurophysiol*. 2007; 98:638–656. [PubMed: 17537902]
15. Dong HW, Swanson LW. Organization of axonal projections from the anterolateral area of the bed nuclei of the stria terminalis. *J Comp Neurol*. 2004; 468:277–298. [PubMed: 14648685]
16. Dumont EC, Williams JT. Noradrenaline triggers GABA inhibition of bed nucleus of the stria terminalis neurons projecting to the ventral tegmental area. *J Neurosci*. 2004; 24:8198–8204. [PubMed: 15385602]
17. Jalabert M, Aston-Jones G, Herzog E, Manzoni O, Georges F. Role of the bed nucleus of the stria terminalis in the control of ventral tegmental area dopamine neurons. *Prog Neuropsychopharmacol Biol Psychiatry*. 2009; 33:1336–1346. [PubMed: 19616054]
18. Kudo T, et al. Three types of neurochemical projection from the bed nucleus of the stria terminalis to the ventral tegmental area in adult mice. *J Neurosci*. 2012; 32:18035–18046. [PubMed: 23238719]

19. Briand LA, Vassoler FM, Pierce RC, Valentino RJ, Blendy JA. Ventral tegmental afferents in stress-induced reinstatement: the role of cAMP response element-binding protein. *J Neurosci*. 2010; 30:16149–16159. [PubMed: 21123561]
20. Christianson JP, et al. Safety signals mitigate the consequences of uncontrollable stress via a circuit involving the sensory insular cortex and bed nucleus of the stria terminalis. *Biol Psychiatry*. 2011; 70:458–464. [PubMed: 21684526]
21. Mahler SV, Aston-Jones GS. Fos activation of selective afferents to ventral tegmental area during cue-induced reinstatement of cocaine seeking in rats. *J Neurosci*. 2012; 32:13309–13326. [PubMed: 22993446]
22. Boyden ES, Zhang F, Bamberg E, Nagel G, Deisseroth K. Millisecond-timescale, genetically targeted optical control of neural activity. *Nat Neurosci*. 2005; 8:1263–1268. [PubMed: 16116447]
23. Fuller JH, Schlag JD. Determination of antidromic excitation by the collision test: problems of interpretation. *Brain Res*. 1976; 112
24. Sparta DR, et al. Construction of implantable optical fibers for long-term optogenetic manipulation of neural circuits. *Nat Protoc*. 2012; 7:12–23. [PubMed: 22157972]
25. Nagy FZ, Pare D. Timing of impulses from the central amygdala and bed nucleus of the stria terminalis to the brain stem. *J Neurophysiol*. 2008; 100:3429–3436. [PubMed: 18971295]
26. Vong L, et al. Leptin action on GABAergic neurons prevents obesity and reduces inhibitory tone to POMC neurons. *Neuron*. 2011; 71:142–154. [PubMed: 21745644]
27. Stuber GD, et al. Excitatory transmission from the amygdala to nucleus accumbens facilitates reward seeking. *Nature*. 2011; 475:377–380. [PubMed: 21716290]
28. Erb S, Shaham Y, Stewart J. Stress-induced relapse to drug seeking in the rat: role of the bed nucleus of the stria terminalis and amygdala. *Stress*. 2001; 4
29. Poulos AM, Ponnusamy R, Dong HW, Fanselow MS. Compensation in the neural circuitry of fear conditioning awakens learning circuits in the bed nuclei of the stria terminalis. *Proc Natl Acad Sci U S A*. 2010; 107:14881–14886. [PubMed: 20679237]
30. Phelps EA, LeDoux JE. Contributions of the amygdala to emotion processing: from animal models to human behavior. *Neuron*. 2005; 48:175–187. [PubMed: 16242399]

### Additional references

31. Roitman MF, Wheeler RA, Carelli RM. Nucleus accumbens neurons are innately tuned for rewarding and aversive taste stimuli, encode their predictors, and are linked to motor output. *Neuron*. 2005; 45:587–597. [PubMed: 15721244]
32. Tye KM, Janak PH. Amygdala neurons differentially encode motivation and reinforcement. *J Neurosci*. 2007; 27:3937–3945. [PubMed: 17428967]

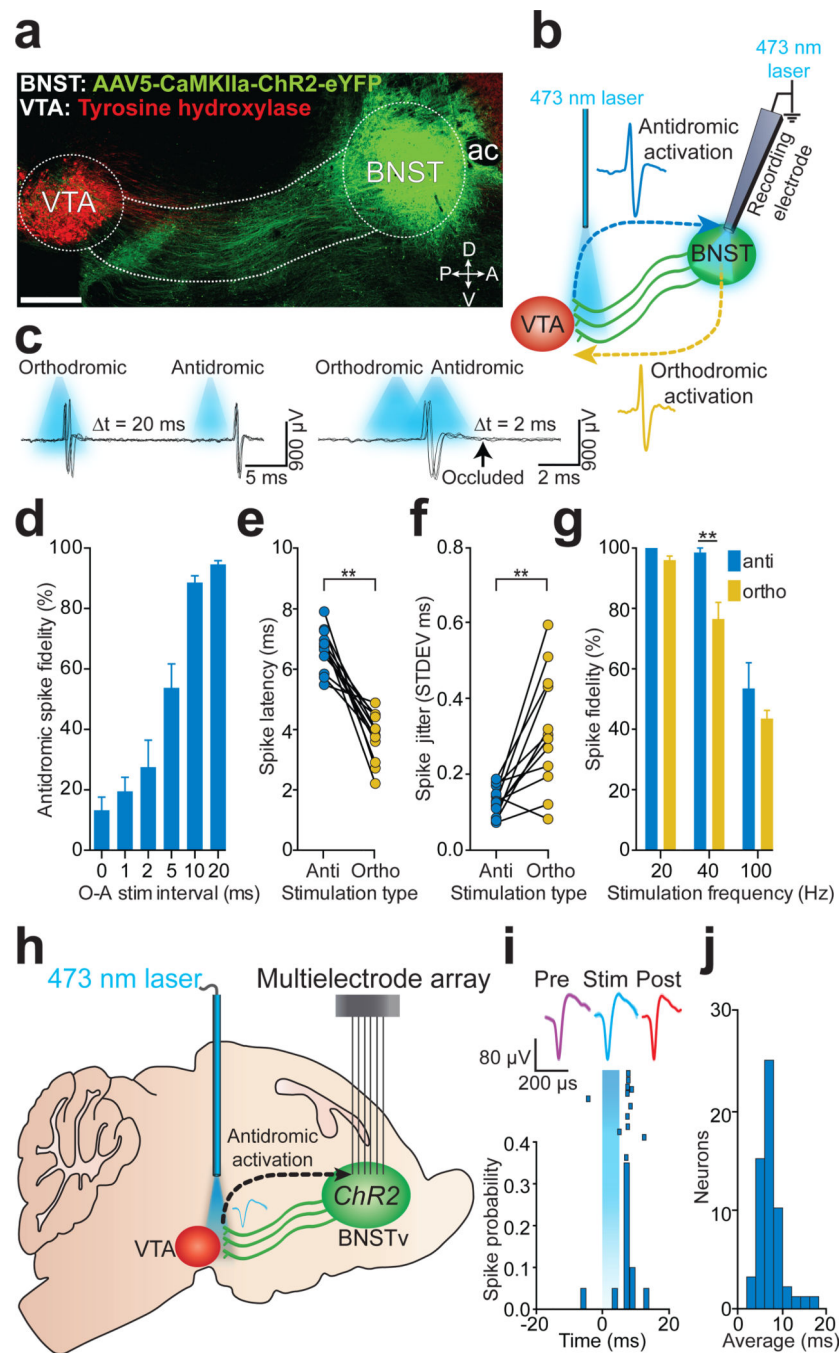


**Figure 1. Optogenetic identification of BNSTv→VTA projection neurons**

**a.** Sagittal image showing the BNSTv→VTA projection (ac, anterior commissure; D, dorsal; V, ventral; P, posterior; A, anterior; scale = 500  $\mu$ m). **b.** Optogenetic collision test. **c.** Example traces from a single CaMKIIa<sup>BNSTv→VTA</sup> unit demonstrating antidromic-orthodromic spike collision. **d.** Significant reduction in antidromic spike fidelity (%) at short antidromic-orthodromic photostimulation intervals (O, orthodromic photostimulation; A, antidromic photostimulation;  $F_{5,65} = 48.63$ ,  $P < 0.0001$ ;  $n = 12$  units). **e.** Antidromic spike latencies were significantly greater than orthodromic latencies ( $P < 0.0001$ ;  $n = 12$  units). **f.**

Antidromic-initiated spikes displayed significantly greater latency stability compared to orthodromic-activated spikes ( $P < 0.001$ ;  $n = 12$  units). **g.** Antidromic spikes responded more reliably to 40 Hz photostimulation compared to orthodromic spikes ( $F_{2,18} = 11.2$ ,  $P = 0.003$ ,  $n = 4$  units). **h.** Optogenetic identification of BNSTv→VTA projection neurons in behaving mice. **i.** Representative peri-event histogram and raster of a single unit timelocked to 5 ms antidromic photostimulation. **j.** Mean first-spike latencies following antidromic photostimulation for all identified CaMKIIa<sup>BNSTv→VTA</sup> projection neurons ( $n = 53$  units,  $n = 7$  mice). All values for all figures represent mean  $\pm$  s.e.m. \*  $P < 0.05$ , \*\*  $P < 0.01$ .

Author Manuscript

Author Manuscript

Author Manuscript

Author Manuscript

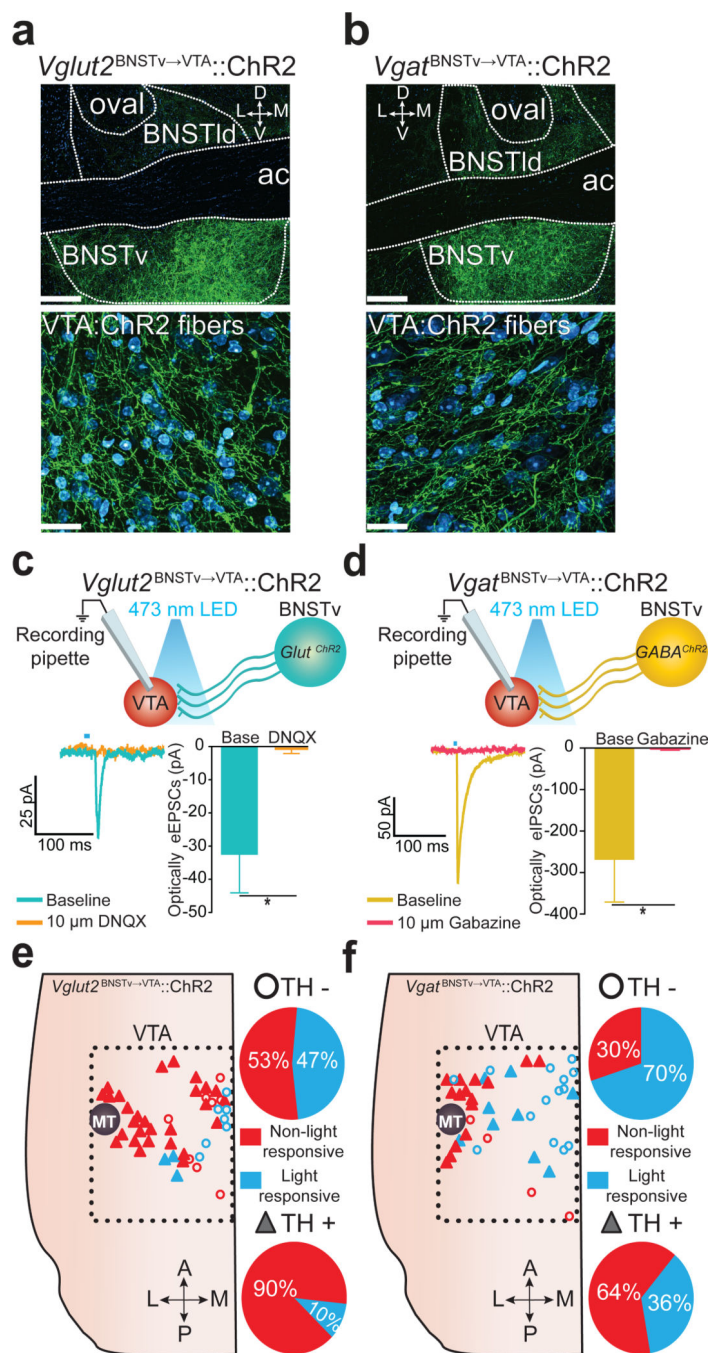


**Figure 2. Excitatory and inhibitory synapses onto non-dopaminergic VTA neurons from neurochemically distinct BNSTv neurons**  
**a – b.** ChR2-eYFP in the BNSTv (top) and fibers in the VTA (bottom) in *Vglut2-ires-cre* (**a**) and *Vgat-ires-cre* (**b**) mice (BNSTld, lateral-dorsal BNST; oval, oval nucleus BNST; D, dorsal; V, ventral; L, lateral; M, medial; green = ChR2-eYFP; cyan = fluorescent Nissl stain; scale bars = 200  $\mu$ m (top), 20  $\mu$ m (bottom)). **c.** Optically-evoked EPSCs recorded in VTA neurons following *Vglut2*<sup>BNSTv→VTA::ChR2</sup> stimulation before and after application of the glutamate receptor antagonist, DNQX (bottom) ( $n = 4$  cells,  $P = 0.0307$ ). **d.** Optically-

evoked IPSCs recorded in VTA neurons following  $Vgat^{BNSTv \rightarrow VTA::ChR2}$  stimulation before and after application of the GABA<sub>A</sub> receptor antagonist, Gabazine (bottom) ( $n = 4$  cells,  $P = 0.0378$ ). **e - f.** Location of light-responsive and non light-responsive dopaminergic and non-dopaminergic neurons in horizontal VTA slices following photostimulation of  $Vglut2^{BNSTv \rightarrow VTA::ChR2}$  (**e**) and  $Vgat^{BNSTv \rightarrow VTA::ChR2}$  (**f**) projections. \*  $P < 0.05$ .

Author Manuscript

Author Manuscript

Author Manuscript

Author Manuscript

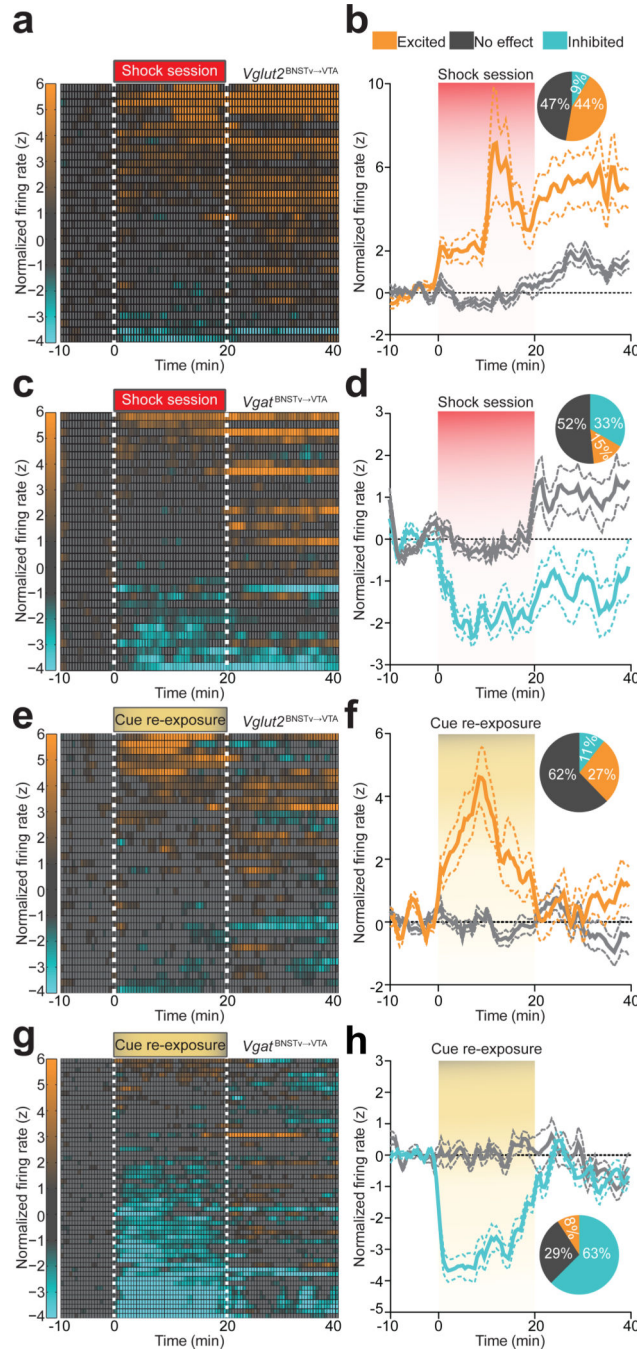


**Figure 3.  $Vglut2^{BNSTv \rightarrow VTA}$  and  $Vgat^{BNSTv \rightarrow VTA}$  projection neurons display distinct firing patterns in response to foot shock and shock-associated contextual cues**

**a.** Color-coded normalized firing rates for all identified  $Vglut2^{BNSTv \rightarrow VTA}$  neurons in response to the first foot-shock session. **b.** Average normalized firing rate of classified shock-excited  $Vglut2^{BNSTv \rightarrow VTA}$  neurons is significantly altered compared to no effect classified neurons during and following the foot-shock session ( $F_{99,2900} = 3.13$ ,  $P < 0.0001$ ,  $n = 34$  units,  $n = 7$  mice). Inset: percentages of classified neurons. **c.** Color-coded normalized firing rates for all identified  $Vgat^{BNSTv \rightarrow VTA}$  neurons in response to the first

foot-shock session. **d.** Average normalized firing rate of classified shock-inhibited  $Vgat^{BNSTv \rightarrow VTA}$  neurons is significantly altered compared to no effect classified neurons during and following the foot-shock session ( $F_{99,2600} = 2.66$ ,  $P < 0.0001$ ,  $n = 33$  units,  $n = 5$  mice). **e.** Color-coded normalized firing rates of identified  $Vglut2^{BNSTv \rightarrow VTA}$  neurons in response to cue re-exposure. **f.** Average normalized firing rate of classified cue-excited  $Vglut2^{BNSTv \rightarrow VTA}$  neurons is significantly altered compared to no effect classified neurons during and following cue re-exposure ( $F_{99,3100} = 5.135$ ,  $P < 0.0001$ ,  $n = 37$  units,  $n = 4$  mice). **g.** Color-coded normalized firing rates of  $Vgat^{BNSTv \rightarrow VTA}$  neurons in response to cue re-exposure. **h.** Average normalized firing rate of classified cue-inhibited  $Vgat^{BNSTv \rightarrow VTA}$  neurons is significantly altered compared to no effect classified neurons during and following cue re-exposure ( $F_{99,4900} = 8.285$ ,  $P < 0.0001$ ,  $n = 56$  units,  $n = 4$  mice).

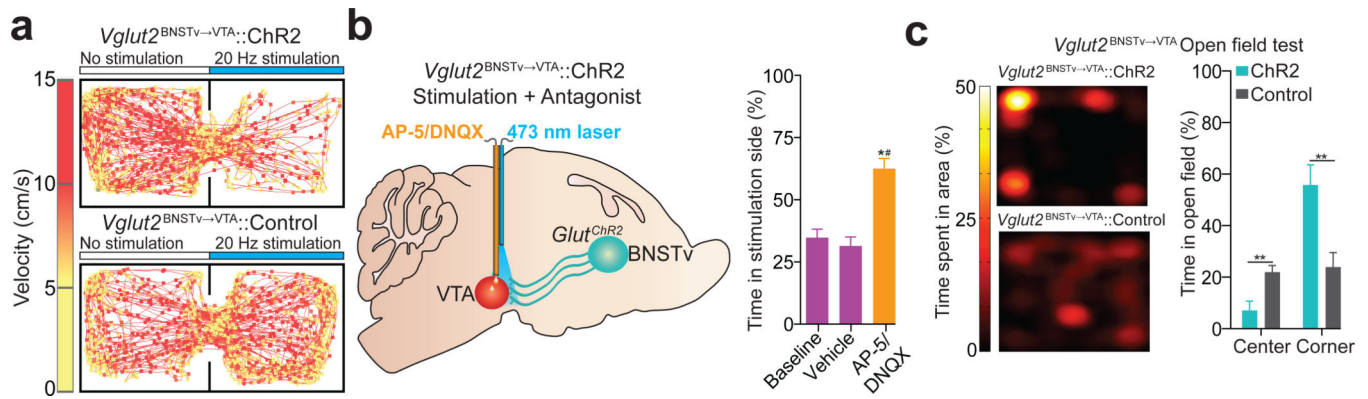


**Figure 4. Photostimulation of the *Vglut2*<sup>BNSTv→VTA</sup> pathway promotes aversion and anxiety**  
**a.** Representative real-time place preference tracks from *Vglut2*<sup>BNSTv→VTA::ChR2</sup> (top) and control (bottom) mice. **b.** Intra-VTA infusions of a glutamate antagonist cocktail, followed by *Vglut2*<sup>BNSTv→VTA::ChR2</sup> stimulation during real-time place preference blocked aversion ( $F_{3,15} = 12.811$ ,  $P < 0.001$ ,  $n = 6$  mice). **c.** Representative heat maps displaying average time spent in an open field for 10 min following stimulation from *Vglut2*<sup>BNSTv→VTA::ChR2</sup> (top) and *Vglut2*<sup>BNSTv→VTA::Control</sup> (bottom) mice. *Vglut2*<sup>BNSTv→VTA::ChR2</sup> mice spent significantly more time in the corners ( $P = 0.008$ ) and less time in the center ( $P = 0.007$ ) of an open field immediately following constant 20 Hz stimulation compared to *Vglut2*<sup>BNSTv→VTA::Control</sup> mice ( $n = 6$  mice per group).

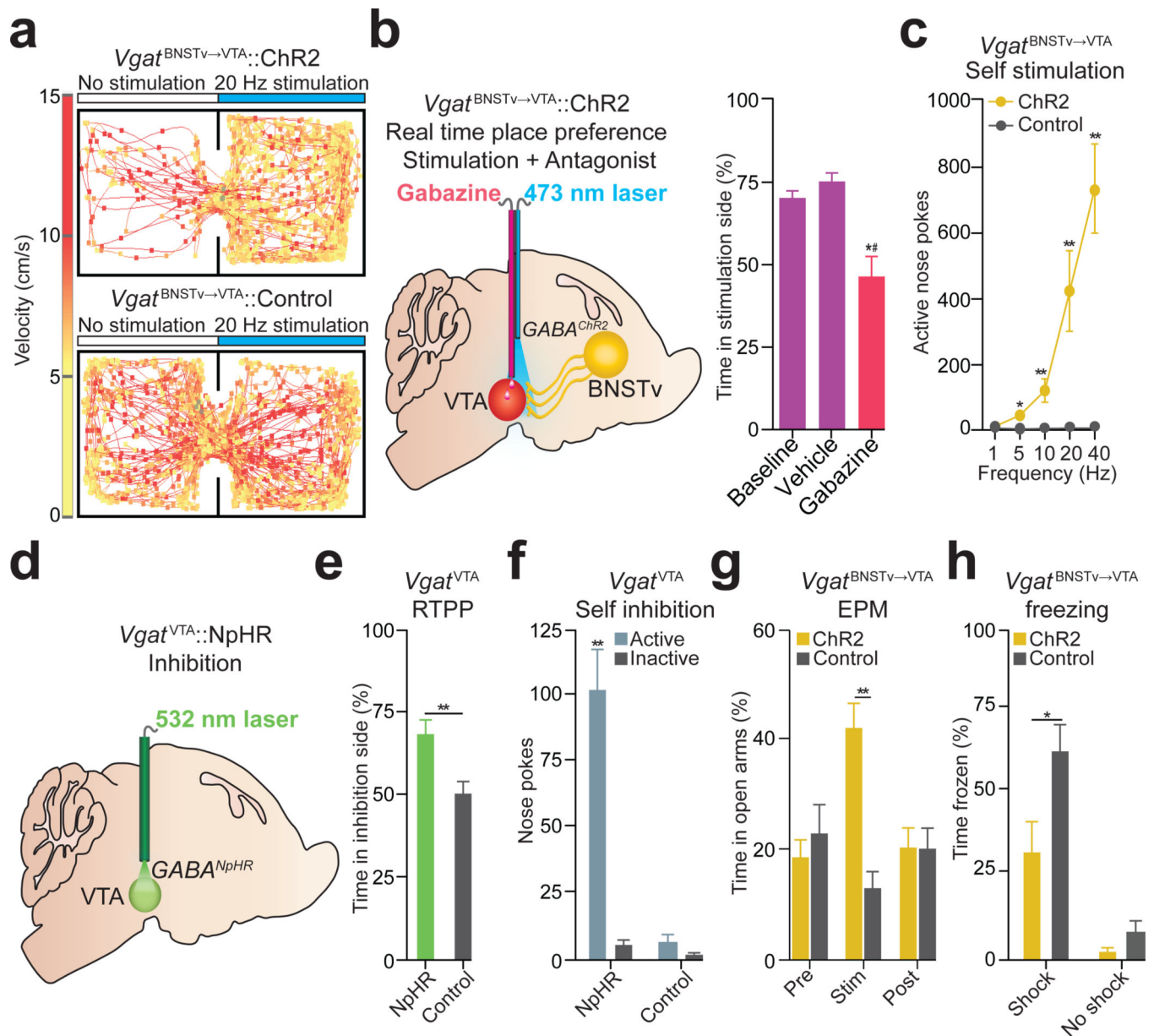


**Figure 5. Photostimulation of the  $Vgat^{BNSTv \rightarrow VTA}$  pathway and inhibition of  $Vgat^{VTA}$  neurons produces reward-related behaviors and attenuates anxiety**

**a.** Real-time place preference representative tracks from  $Vgat^{BNSTv \rightarrow VTA}::ChR2$  (top) and control (bottom) mice. **b.** Intra-VTA infusions of the  $GABA_A$  antagonist, Gabazine, followed by  $Vgat^{BNSTv \rightarrow VTA}::ChR2$  stimulation abolished place preference ( $F_{3,15} = 13.718$ ,  $P < 0.001$ ,  $n = 6$  mice) **c**  $Vgat^{BNSTv \rightarrow VTA}::ChR2$  mice made significantly more nose pokes to obtain photostimulation compared to controls ( $F_{4,36} = 12.42$ ,  $P < 0.001$ ,  $n = 5 - 7$  mice per group). **d.** Schematic detailing  $Vgat^{VTA}::NpHR$  inhibition during behavioral experiments. **e**  $Vgat^{VTA}::NpHR$  mice spent significantly more time in the inhibition-paired side when compared to controls ( $P = 0.01$ ,  $n = 6$  mice per group). **f**  $Vgat^{VTA}::NpHR$  mice made significantly more nose pokes to obtain photoinhibition compared to controls ( $P < 0.001$ ,  $n = 5$  mice per group). **g**  $Vgat^{BNSTv \rightarrow VTA}::ChR2$  mice spent significantly more time

in the elevated-plus maze (EPM) open arms compared to controls during the 5 min photostimulation epoch ( $F_{2,24} = 14.648$ ,  $P < 0.001$ ,  $n = 7$  mice per group). **f.** After concurrent photostimulation during the foot-shock session,  $Vgat^{BNSTv \rightarrow VTA::ChR2}$  mice ( $n = 6 - 7$ ) spent significantly less time frozen compared to controls ( $F_{1,22} = 37.992$ ,  $P < 0.001$ ). \*  $P < 0.05$ , \*\*  $P < 0.01$ , \*# $P$  significant compared to all manipulations.

Author Manuscript

Author Manuscript

Author Manuscript

Author Manuscript